

1
2
3
4
5
6
7
8
9
10
11
12
13
14
15
16
17
18

Prenatal alcohol exposure disrupts Shh pathway and primary cilia genes in the mouse neural tube

Karen E. Boschen¹, Eric W. Fish¹, & Scott E. Parnell^{1,2*}

¹Bowles Center on Alcohol Studies, University of North Carolina, Chapel Hill, NC, USA

²Department of Cell Biology and Physiology, University of North Carolina, Chapel Hill, NC, USA

* Corresponding author: Scott E. Parnell, Ph.D.

Email: sparnell@med.unc.edu (SEP)

19 **Abstract**

20 Neurulation-stage alcohol exposure (NAE; embryonic day [E] 8-10) is associated with midline
21 craniofacial and CNS defects that likely arise from disruption of morphogen pathways, such as Sonic
22 hedgehog (Shh). Notably, midline anomalies are also a hallmark of genetic ciliopathies such as Joubert
23 syndrome. We tested whether NAE alters Shh pathway signaling and the number and function of
24 primary cilia, organelles critical for Shh pathway transduction. Female C57BL/6J mice were
25 administered two doses of alcohol (2.9 g/kg/dose) or vehicle on E9. Embryos were collected 6, 12, or
26 24 hr later, and changes to Shh, cell cycle genes, and primary cilia were measured in the rostroventral
27 neural tube (RVNT). Within the first 24 hours post-NAE, reductions in Shh pathway and cell cycle gene
28 expression and the ratio of Gli3 forms in the full-length activator state were observed. RVNT volume
29 and cell layer width were reduced at 12 hr. In addition, expression of multiple cilia-related genes were
30 observed at 6 hr post-NAE. As a further test of cilia gene-ethanol interaction, mice heterozygous for
31 *Kif3a* exhibited perturbed behavior during adolescence following NAE compared to vehicle-treated
32 mice, and *Kif3a* heterozygosity exacerbated the hyperactive effects of NAE on exploratory activity.
33 These data demonstrate that NAE downregulates the Shh pathway in a region of the neural tube that
34 gives rise to alcohol-sensitive brain structures and identifies disruption of primary cilia function, or a
35 “transient ciliopathy”, as a possible cellular mechanism of prenatal alcohol pathogenesis.

36 Introduction

37 Prenatal alcohol exposure is the leading cause of preventable birth defects in the US, with Fetal
38 Alcohol Spectrum Disorders (FASD) estimated to affect at least 5% of live births each year (1). Alcohol
39 exposure often occurs before pregnancy is identified, during the early, important stages of embryonic
40 development, such as gastrulation and neurulation. Early gestational alcohol exposure has been linked
41 to growth retardation, central nervous system dysfunction, and distinct craniofacial malformations,
42 including the “classic” facial phenotype of Fetal Alcohol Syndrome (FAS) characterized by midline
43 defects such as hypotelorism and an absent philtrum (2, 3), as well as more subtle facial variances (4).
44 Alcohol exposure during gastrulation, the stage when the embryo first forms distinct cell layers (3rd
45 week in humans, embryonic day [E] 7 in mice), induces widespread cell death in the neuroectoderm
46 (5), and subsequent diminished Sonic hedgehog (Shh) signaling as a pathogenic mechanism for
47 gastrulation-stage alcohol exposure (6-10). Alcohol exposure during neurulation, as the neural tube
48 forms and closes (~4th-5th weeks in humans, E8-10 in mice), produces midline structural defects in
49 brain regions such as the hypothalamus, ventricles, pituitary, and septal regions (11-14). However,
50 while prenatal alcohol exposure during neurulation causes cell death in regions such as the
51 rhombencephalon, alcohol-induced apoptosis is not as pronounced in the rostroventral neural tube (5),
52 the portion of the neural tube that gives rise to ventral midline brain structures.

53 The Shh signaling pathway is transduced within immotile sensory organelles known as primary
54 cilia (15, 16). Genetic disruption of the function and/or stability of primary cilia induces several
55 developmental abnormalities, exemplified by the ciliopathy diseases, such as Joubert syndrome.
56 Genetic ciliopathies cause multiple organ system defects, ocular malformations, cleft palates and lips,
57 holoprosencephaly, and polydactyly (17, 18). Abnormal Shh signaling has been reported in cultured
58 cells collected from humans with gene mutations linked to ciliopathies (19, 20) and knockdown of *Kif3a*,
59 or other intraflagellar transport proteins in mouse models of ciliopathies disrupts the Shh pathway (21-
60 23) and causes Gli-dependent midfacial defects (24-26).

61 We hypothesized that neurulation-stage alcohol exposure (NAE) also disrupts Shh signaling in
62 the rostroventral region of the neural tube (RVNT) that gives rise to many of the affected midline brain
63 structures, explaining the manifestation of subtle craniofacial and CNS defects associated with alcohol
64 exposure during this developmental window. We tested the effect of mid-neurulation (E9.0) alcohol
65 exposure on expression of the *Shh* pathway and cell cycle genes within 24 hr following exposure.
66 Following determination that NAE significantly decreased Shh and cell cycle gene expression, we were
67 interested in whether neurulation-stage alcohol also affects primary cilia, as Shh transduction takes
68 place within the primary cilia. To test this hypothesis, we analyzed the density of primary cilia in the
69 RVNT and expression of genes known to play a role in cilia protein trafficking and ciliogenesis. Finally,
70 we studied whether NAE interacts with cilia function to increase the sensitivity to the long-term effects
71 of NAE. For this experiment, we exposed embryonic mice with a partial deletion of the key cilia gene
72 *Kif3a*, which is a well-characterized mouse model of genetic ciliopathies, to E9.0 alcohol and then
73 measured adolescent behavioral performance on tasks known to be affected by prenatal alcohol.

74 **Methods and Materials**

75 **Animals**

76 Male and female adult C57BL/6J mice were obtained from Jackson Laboratories (Stock No: 000664;
77 Bar Harbor, ME). Males were housed singly and females were housed in groups of up to five per
78 standard polycarbonate cage with cob bedding, a shelter, and nesting material. All mice had *ad libitum*
79 access to food (Prolab Isopro RMH 3000, LabDiet, St. Louis, MO) and water, and were maintained on a
80 12:12 hr light/dark cycle. For mating, 1-2 female mice were placed into the cage of a male for 1-2 h and
81 were checked for a vaginal plug to confirm copulation. E0.0 was defined as the beginning of the mating
82 session when the plug was found. Mated females were weighed and housed in a clean cage with up to
83 5 mice. All experimental procedures and euthanasia protocols were approved by the Institutional Care
84 and Use Committee (IACUC) at University of North Carolina (approval #18-203).

85 For behavior studies, male *Kif3a*^{+/-} (B6.129-Kif3a^{tm1Gsn}/J, Stock No: 003537; Jackson
86 Laboratories, Bar Harbor, ME) and female C57BL/6J mice were obtained, housed, and mated as
87 described above to produce *Kif3a*^{+/+} and *Kif3a*^{+/-} offspring. Generation of *Kif3a*^{-/-} mice was avoided as
88 this mutation is embryonically lethal. All dams were singly housed in clean cages on E15. Alcohol- and
89 vehicle-treated litters (see below) were housed with their dams, culled to a maximum of 8 pups/litter at
90 postnatal day (PD) 3, weighed, ear marked, and tail-clipped for genotyping on PD14, and left
91 undisturbed until weaning at PD28 when they were housed in same sex groups with their littermates.
92 All the mice from each litter were tested on behavioral experiments conducted between PD28–33 by an
93 experimenter who was unaware of the prenatal treatments and *Kif3a* genotype.

94 **Neurulation-stage alcohol exposure (NAE)**

95 On E9.0, pregnant dams were administered two doses of ethanol (25% vol/vol ethyl alcohol,
96 Pharmaco-Aaper, Brookfield, CT, at a dose of 2.9 g/kg) in Lactated Ringer's solution 4 hr apart via
97 intraperitoneal (i.p.) injection. These mice were designated as the NAE group. A separate group of mice
98 were administered an equal volume of vehicle (1.5 ml/100 g body weight). This model of alcohol
99 exposure has been previously shown to result in maternal blood alcohol concentrations of ~400 mg/dl
100 (27). For molecular studies, dams were humanely sacrificed via CO₂ followed by cervical dislocation
101 either 6, 12, or 24 hr after the first ethanol injection. Embryos were dissected out and placed into cold
102 RNase-free Dulbecco's saline solution. For all assays, embryos were stage-matched based on somite
103 number (E9.25: 21-22 somites, E9.5: 24-25 somites, E10: 30-31 somites). A maximum of two embryos
104 per litter were used in each assay to minimize litter effects.

105 **Embryo immunohistochemistry**

106 The chorion and amnion were removed from all embryos and placed into 4% paraformaldehyde
107 for ~72 h. Stage-matched embryos were then processed for paraffin-embedding on a Leica tissue
108 processing station and sectioned at 7 μm on a microtome. A total of 6-10 sections per embryo,
109 encompassing the rostroventral neural tube (RVNT), were processed for immunohistochemistry. Briefly,

110 paraffin residue was dissolved in xylenes and sections were rehydrated in ethanol washes. Slides were
111 quenched in 10% H_2O_2 /90% methanol for 10 min and incubated for 30 min in 10% Citra Plus Buffer
112 (BioGeneX, Fremont, CA) in a steam chamber. The slides were then blocked in normal goat
113 serum/Triton-X/bovine serum albumin blocking solution for 1 hr and incubated overnight with primary
114 antibody (Arl13b, 1:500, NeuroMabs, University of California-Davis) at 4°C for 24 h. Slides were then
115 incubated with secondary antibody (anti-mouse Alexafluor 488, 1:1000, Thermofisher, Waltham, MA)
116 for 2 hr at room temperature and cover slipped with Vectashield HardSet Antifade Mounting Medium
117 with DAPI (Vector, Burlingame, CA).

118 **Confocal imaging and image quantification**

119 Cilia were imaged on a Zeiss 880 confocal microscope with a 40x oil lens. Image stacks were
120 obtained at a step of 0.46 μm between images. Stacks were then compressed into a single image
121 containing a depth color code with Fiji (ImageJ) software (28). Cilia within the known volume of the
122 RVNT were counted with the Cell Counter plug-in and expressed as number of cilia per 100 μm^3 . RVNT
123 volume and cell layer width were determined using images of the same sections taken with a 10x lens.
124 The DAPI-labeled cell layer was traced to obtain volumetric measurements and the cell layer width was
125 measured at multiple points within each RVNT (2 measurements per slide) using Fiji software.

126 **Gene expression assays**

127 The RVNT of stage-matched embryos were dissected and placed into lysis buffer and stored at
128 -80°C until processing. RNA was isolated from the supernatant using the RNeasy Plus Micro Kit
129 (Qiagen, Valencia, CA). Nucleic acid concentration and quality were determined using the Qubit 3.0
130 fluorometer and Nanodrop 2000 (Thermofisher, Waltham, MA). Generation of cDNA used a consistent
131 starting amount of RNA across all embryos (100 ng). Multiplex qRT-PCR was used to determine
132 alcohol-induced gene expression changes (n = 6-10 embryos/treatment). Taqman probes (Invitrogen)
133 and Taqman Multiplex PCR mix (Applied Biosystems) were used to determine expression changes in
134 the following genes: *Shh* (Mm00436528), *Gli1* (Mm00494654), *Gli2* (Mm01293117), *Ccdn1*

135 (Mm00432359), *Ccdn2* (Mm00438071), *Fgf15* (Mm00433278), *Cep41* (Mm00473478), *Hap1*
136 (Mm00468825), *Rilpl2* (Mm01199587), *Evc* (Mm00469587), *Nek4* (Mm00478688), and *Dpcd*
137 (Mm00620237). For all assays, *18s* (Mm03928990) or *Pgk1* (Mm000435617) were used as reference
138 genes. Reference genes were confirmed to be unaffected by prenatal treatment in separate embryos
139 prior to use in these experiments. However, *18s* expression showed high baseline variability in the
140 E9.25 embryos, leading to the use of *Pgk1* as a reference gene for this time point. All reactions were
141 run in triplicate and amplicon specificity was confirmed with gel electrophoresis.

142 **Western Blot**

143 RVNT's of each litter (n = 5-10 samples per tube) were pooled and lysed in RIPA buffer with 1X
144 Halt protease and phosphatase inhibitors (Thermofisher, Waltham, MA) in order to obtain sufficient
145 protein for western blot analyses. For E9.25, 5 vehicle and 6 NAE litters were used, and for E9.5, 6
146 vehicle and 7 NAE litters were used. Protein concentrations were determined with the Micro BCA kit
147 (Thermofisher, Waltham, MA) and colorimetrics measured at 540 nm on a spectrophotometer. 15 µg of
148 sample with 4X Laemmli sample buffer were added to each lane of a tris-glycine gel in 1X TGX running
149 buffer and run at 150V for 45 min. Protein weights were determined with the Dual Color protein ladder
150 (Bio-Rad, Hercules, CA). Proteins were transferred to a membrane using the iBlot2 system and
151 incubated overnight at 4°C with primary antibody (anti-Gli3, 1:500, AF3690, R&D Systems,
152 Minneapolis, MN). Membranes were then incubated in secondary antibody (anti-goat Alexafluor 680,
153 1:10,000, Thermofisher, Waltham, MA) for 1 hr at room temperature and imaged on a Licor Odyssey
154 scanner. GAPDH (1:3000, 14C10, Cell Signaling, Danvers, MA) was used as an internal loading
155 control. The relative intensities of the Gli3 protein bands (Gli3^{FL} [~190 kDa] and Gli3^{REP} [~83 kDa]) were
156 analyzed with ImageJ Gel Analyzer software and normalized to internal control bands. The ratio of
157 Gli3^{FL}: Gli3^{REP} forms was calculated and expressed as a percentage of total Gli3.

158 **Adolescent behavioral procedures**

159 All the mice from each litter generated from the mating of a *Kif3a*^{+/-} male and C57BL/6J female
160 (n = 16 litters vehicle-exposed and 19 litters NAE) were tested on behavioral experiments conducted
161 between PD28–33 by an experimenter unaware of the prenatal treatments and *Kif3a* genotype. The
162 experiments were conducted in the UNC Behavioral Phenotyping Core during the light portion of the
163 12:12hr light:dark schedule. All mice were tested in the following testing order: rotarod trials 1-3;
164 elevated plus maze (EPM); open-field; rotarod trials 4 and 5. The EPM was tested before the open field
165 to minimize potential carry-over effects, as the EPM is more sensitive to the effects of prior testing
166 history (29, 30). Technical issues during testing resulted in two male animals being excluded from the
167 EPM and one male from open field analyses.

168 The rotarod (Ugo-Basile, Stoelting Co., Wood Dale, IL) measured the latency to fall off or rotate
169 around the top of a dowel which progressively accelerated from 3 rpm to 30 rpm during the maximum of
170 a 5-min test, conducted during three repeated trials on the first day of testing and two repeated trials on
171 the second day of testing. Each trial was separated by ~45 sec. The EPM was 50 cm above the floor
172 and contained two open arms (30 cm length, 220 lux) and two closed arms (20 cm high walls, 120 lux).
173 During the 5-min test, an observer recorded the number of entries and time spent in each of the arms.
174 These data were used to calculate the percent of open arm time [(open arm time/total arm time) x 100],
175 the total arm entries, and the percent of open arm entries [(open arm entries/total arm entries) x 100].
176 The open field (41 x 41 x 30 cm) was illuminated (120 lux at the edges, 150 lux in the center), housed
177 within a sound-attenuated chamber and equipped with upper and lower grids of photobeams for the
178 detection of horizontal and vertical activity and position of the mouse (Versamax System: Accuscan
179 Instruments, Columbus, OH). The open field was conducted over 60 min and the primary measures
180 were horizontal activity, total distance traveled, time spent in the center of the chamber, and distance
181 traveled in the center. Number of rears and rotations were also recorded. Open field data were
182 analyzed as four separate 15-min epochs (i.e. min 0-15, min 16-30, min 31-45, and min 46-60), based
183 on prior findings that the initial minutes of the open field test are most sensitive to developmental drug
184 exposure (11, 31).

185 **Adolescent brain measurements**

186 Following completion of behavioral tasks on PD37, mice were deeply anesthetized with
187 tribromoethanol anesthesia and transcardially perfused with 1X PBS followed by 10% formalin. Brains
188 were removed and stored in formalin for at least one week. Prior to paraffin embedding, fixed whole
189 brains were cleared by rocking at room temperature in 1X PBS for one week and 70% ethanol for one
190 week (each solution changed daily). Brains were then cut into two sections, the frontal lobes and
191 cerebellum, and paraffin-embedded on a Leica tissue processing station. Tissue was then embedded in
192 paraffin block and sectioned at 10 μm on a microtome. Every 5th slide (containing 3-4 sections per
193 slide) throughout the entirety of the cortex was stained using cresyl violet. One section per slide was
194 imaged and the ventricles traced using Fiji/ImageJ (28). Total area of the ventricles were summed per
195 section and averaged across the entire brain. For midline brain width and medial height, lines were
196 drawn across images of one section of each slide throughout the cortex and measured in Fiji. Midline
197 brain width was measured at the widest part of the cortex (dorsal/ventral bregma \sim 3.0) and height was
198 measured as close to the midline as possible (medial/lateral bregma 0.25); measurements were
199 averaged across the entire brain.

200 **Statistical analyses**

201 Cilia number, RVNT volume, and Western blot band intensity were analyzed using unpaired *t*-
202 tests comparing prenatal treatment (NAE vs. vehicle) at each time point with Welch's correction when
203 necessary. The Benjamini-Hochberg correction was used if multiple unpaired *t*-tests were run within an
204 experiment (false discovery rate = 0.10) (32). Raw *p*-values shown in tables and in the text remain
205 statistically significant following correction unless otherwise noted. Multiplex qRT-PCR gene expression
206 data are expressed as log₂ fold change calculated using the $2^{(-\Delta\Delta\text{CT})}$ method (33). Data were analyzed
207 using either unpaired *t*-tests with corrected *p*-values (cilia-related genes) or two-way ANOVAs
208 (Treatment x Time Point) with corrected *t*-tests run as *post hoc*s for analyses with significant
209 interactions (Shh path genes, Gli3, cell cycle genes). For behavior assays, litter means were analyzed

210 for each treatment and genotype to control for between litter effects (34). Males and females were
211 analyzed separately, because our previous studies demonstrated sex differences on these measures
212 (12, 35). EPM data were analyzed using two-way ANOVAs (treatment x genotype) and open field and
213 rotarod data were analyzed with three-way ANOVAs (treatment x genotype x time bin or trial). For the
214 behavioral analysis, we predicted, *a priori*, that any effects of NAE or *Kif3a*^{+/-} would be exaggerated
215 when these treatments were combined, in other words, that the NAE *Kif3a*^{+/-} mice would have the
216 largest difference from the vehicle-treated *Kif3a*^{+/+} mice. Ventricle area measurements were analyzed
217 using a three-way ANOVA (treatment x genotype x bregma), while width and height measurements
218 were analyzed with two-way ANOVAs (treatment x genotype). *Post hoc* analyses were conducted when
219 appropriate. Statistical differences were considered significant at an adjusted *p*-value threshold of 0.05.

220 Results

221 NAE downregulates expression of the Shh pathway in the RVNT

222 Previous work has demonstrated that the shape and size of the ventricles, pituitary, and
223 hypothalamus are altered following NAE (11-14), suggesting that during neurulation the RVNT (from
224 which these structures are derived) is particularly vulnerable to alcohol. Dysregulation of Shh signaling
225 within the RVNT is likely a mechanism for structural changes to midline brain regions following NAE,
226 however, this hypothesis has never been tested (36). To determine whether NAE alters the Shh
227 pathway in the RVNT, we administered two doses of 2.9 g/kg alcohol during mid-neurulation (E9.0) to
228 model binge-like alcohol exposure. We collected the RVNT of stage-matched embryos 6, 12, and 24 hr
229 later (E9.25, E9.5, and E10, see methods for somite numbers) and analyzed *Shh*, *Gli1*, and *Gli2* gene
230 expression. For each gene, two-way ANOVAs were run using the factors of Treatment x Time point
231 (statistics in Table 1), with *post hoc t*-tests between NAE and Veh groups performed for each time point
232 in the event of a significant interaction. First, we found main effects of Treatment and Time Point and a
233 significant interaction for *Shh* gene expression. *Post hocs* revealed that NAE significantly
234 downregulated *Shh* at both the 6 and 12 hr time points ($t(14) = 2.741$, $p = 0.0159$ and $t(14) = 3.608$, $p =$

235 0.003, respectively; Fig 1A; Table 1), extending previously reported reductions in Shh following
236 gastrulation-stage alcohol (9, 10) and demonstrating that NAE also impairs Shh levels in the RVNT, but
237 is independent of concurrent apoptosis in this region (5). Following Shh activation, Gli1 is rapidly
238 upregulated, whereas Gli2 is constitutively expressed. However, without Shh present, Gli2 is cleaved
239 and tagged within the primary cilium for degradation. Activation of Smoothed (Smo) by Shh
240 deactivates this cilia-mediated cleavage of Gli2 and allows it to be shuttled outside of the cilia to
241 activate downstream genes (37). A main effect of treatment was also found for Gli1, with NAE embryos
242 showing reduced *Gli1* expression compared to controls (Table 1, Fig 1A). No effects of NAE were found
243 for *Gli2* expression. In addition, we measured the relative amounts of the two forms of Gli3 protein 6,
244 12, and 24 hr following the beginning of NAE. In the absence of Shh and with normal cilia functioning,
245 Gli3 is found predominantly in the cleaved repressor form (Gli3^{Rep}). Upon Shh pathway activation, the
246 balance of Gli3^{Rep} to the full-length activator form (Gli3^{FL}) is tipped slightly to the activator form to allow
247 Gli1 and Gli2 to proceed with normal gene transcription, including cell cycle genes such as the cyclin
248 family, as well as having a positive feedback effect on Shh itself (38). A two-way ANOVA revealed a
249 significant Treatment x Time interaction (statistics in Table 1). *Post hoc t*-tests found that NAE led to a
250 significantly shifted ratio at the 12 hr time point, with a higher percentage of Gli3^{Rep} compared to vehicle
251 treatment (65.27% Gli3^{Rep} in NAE vs. 54.7% Gli3^{Rep} in vehicle-treated; Fig 1B; $t_{(11)} = 2.67$, $p = 0.022$).
252 The shift in Gli3 to favor the repressor form at this time point coincides with significant reductions in *Shh*
253 and *Gli1* gene expression, as well as smaller RVNT volumes in NAE embryos (Fig 1). The ratio of
254 Gli3^{FL}:Gli3^{Rep} in the RVNT did not significantly differ from control levels 6 or 24 hr post-NAE (Fig 1B). No
255 difference in total amount of Gli3 was observed between treatment groups at any time point and the
256 amount of Gli3^{Rep} did not significantly differ between the E9.25, E9.5, or E10 vehicle-treated groups
257 ($F_{(2,14)} = 0.967$, $p = 0.401$). Changes to Shh pathway transduction could alter the developmental
258 trajectory of craniofacial and CNS regions derived from the RVNT by affecting normal cell proliferation,
259 resulting in the midline defects observed in mice following NAE.
260

261 **Fig 1. Neurulation-stage alcohol exposure (NAE) decreases *Shh* pathway activation in the RVNT.**

262 A) NAE resulted in downregulation of *Shh* and *Gli1* within 24 hr post-exposure (n = 7-10 embryos per
263 group). *Shh* expression was significantly reduced 6 and 12 hr after NAE. Expression of *Gli2* did not
264 differ. Brackets indicate a significant main effect of prenatal treatment. Gene expression data are the
265 log₂ fold change compared to somite-matched embryos from the vehicle group (expressed as 0 on the
266 graph) ± SEM. B) The relative percentage of Gli3^{Rep} to Gli3^{FL} was significantly higher in NAE embryos
267 (n = 7 litters) compared to the vehicle group (n = 6 litters) 12 hr after exposure. Data are expressed as
268 the average Gli3^{FL} or Gli3^{Rep} band density expressed as a percentage of total Gli3. Below are
269 representative bands of Gli3^{FL} (190 kDa) and Gli3^{Rep} (83 kDa). Full blot and loading control GAPDH (37
270 kDa) can be seen in S1 Fig. * = $p < 0.05$, ** = $p < 0.01$.

271 **Table 1. Statistical results for Shh pathway and cell cycle genes.** Gli3 results refer to protein
 272 quantification of Gli3^{Rep}:Gli3^{FL} ratio. Significant ($p < 0.05$) results are listed in bold.

Gene	Associated protein	Function	Log2 Fold Change	Two-way ANOVA (Treatment x Time Point)
<i>Shh</i>	Sonic Hedgehog	Morphogen, neural patterning	E9.25: -0.87 E9.5: -1.89 E10: 0.29	Treatment: $F(1,43) = 6.637, p = 0.014$ Time Point: $F(2,43) = 3.845, p = 0.029$ Interaction: $F(2,43) = 3.916, p = 0.027$
<i>Gli1</i>	GLI Family Zinc Finger 1	Transcription factor	E9.25: 0.01 E9.5: -0.74 E10: -0.89	Treatment: $F(1,43) = 6.814, p = 0.012$ Time Point: $F(2,43) = 1.956, p = 0.154$ Interaction: $F(2,43) = 2.171, p = 0.126$
<i>Gli2</i>	GLI Family Zinc Finger 2	Transcription factor	E9.25: 0.698 E9.5: 0.035 E10: -0.43	Treatment: $F(1,44) = 0.121, p = 0.73$ Time Point: $F(2,44) = 0.452, p = 0.639$ Interaction: $F(2,44) = 0.662, p = 0.521$
<i>Ccnd1</i>	Cyclin D1	Cell cycle	E9.25: -0.387 E9.5: -0.62 E10: -0.48	Treatment: $F(1,43) = 12.735, p = 0.001$ Time Point: $F(2,43) = 0.232, p = 0.794$ Interaction: $F(2,43) = 0.218, p = 0.805$
<i>Ccnd2</i>	Cyclin D2	Cell cycle	E9.25: -0.3288 E9.5: -0.29 E10: -0.94	Treatment: $F(1,43) = 9.772, p = 0.003$ Time Point: $F(2,43) = 1.7, p = 0.195$ Interaction: $F(2,43) = 1.676, p = 0.199$
<i>Fgf15</i>	Fibroblast Growth Factor 15	Cell growth	E9.25: -1.107 E9.5: -0.25 E10: 0.038	Treatment: $F(1,43) = 5.981, p = 0.019$ Time Point: $F(2,43) = 3.917, p = 0.027$ Interaction: $F(2,43) = 2.272, p = 0.115$
Gli3	GLI Family Zinc Finger 3	Transcription factor		Treatment: $F(1,26) = 0.0974, p = 0.756$ Time Point: $F(2,26) = 0.300, p = 0.743$ Interaction: $F(2,26) = 3.42, p = 0.048$

273

274

275 **NAE downregulates cell cycle gene expression and decreases**

276 **RVNT volume**

277 One of the outputs of the Shh signaling pathway is the expression of cell cycle genes. Based on
278 the observed decreases in *Shh* and *Gli1* gene expression and altered Gli3^{FL}:Gli3^{Rep} following NAE, we
279 hypothesized that NAE would also lead to altered expression of genes involved in regulation of cell
280 proliferation. To assess changes in Shh-mediated gene expression, we analyzed three cell proliferation
281 genes downstream of Shh, Cyclin D1 (*Ccnd1*), Cyclin D2 (*Ccnd2*), and Fibroblast growth factor 15
282 (encoded by *Fgf15*; homologous to *Fgf19* in humans), in the RVNT 6, 12, and 24 hr following NAE.
283 *Ccnd1* and *Ccnd2* regulate progression of the G1 phase of the cell cycle (39) and are regulated by the
284 Shh pathway Gli family of transcription factors (40, 41). Furthermore, *Ccnd1* is important for expansion
285 of ventral neural precursors in the early mouse diencephalon (42). In accordance with the alcohol-
286 induced reductions in *Shh*, significant main effects of treatment were found for *Ccnd1* and *Ccnd2* (Fig
287 2A, Table 1), with NAE embryos displaying reduced expression compared to vehicle-treated embryos.
288 *Fgf15* is dependent on Shh signaling and largely overlaps with *Gli1* in expression patterns early in
289 development (42, 43). Functionally, *Fgf15* promotes cell cycle exit and differentiation of neuronal
290 precursors (44). Main effects of both treatment and time point were seen for *Fgf15* expression (Fig 2A;
291 Table 1), however the NAE-induced reduction in *Fgf15* was most pronounced on E9.25.

292 **Fig 2. NAE decreases expression of Shh-mediated cell proliferation genes in the RVNT and**
293 **reduces RVNT volume.** A) NAE reduced expression of key Shh-mediated genes important for cell
294 proliferation processes (n = 6-10 embryos per group) within 24 hr post-exposure. Brackets indicate
295 main effects of prenatal treatment (Table 1). Gene expression data are the log2 fold change compared
296 to the vehicle group (expressed as 0 on the graph) ± SEM. B) RVNT volume is significantly reduced in
297 NAE embryos (filled bars, n = 7) compared to vehicle-treated embryos (open bars, n= 9) 12 hr after
298 exposure, but did not differ at the other two time points. E10 RVNTs were also significantly larger than
299 both E9.25 and E9.5. C) Cell layer width did not differ based on prenatal treatment but did increase

300 over time, with E10 embryos exhibiting wider RVNT cell layers compared to both E9.25 and E9.5
301 embryos. D) Representative images of the RVNT of E9.5 vehicle-treated vs. NAE embryos taken with a
302 10x lens. Scale bar = 100 μm . * = $p < 0.05$, ** = $p < 0.01$, *** = $p < 0.001$, **** = $p < 0.0001$, all values
303 expressed as mean + SEM.

304 Given the disruption of cell cycle-related gene expression, we next analyzed the volume of the
305 RVNT 6, 12, and 24 hr after NAE to examine how the size of this region changed over time and in
306 response to alcohol (Fig 2B). Images taken from the RVNT were obtained at 40x for volumetric
307 analyses; section thickness was also measured at 40x. A significant time (hours post-exposure) x
308 treatment interaction was observed ($F_{(2,39)} = 6.164$, $p = 0.0047$), as well as main effects of both time
309 ($F_{(2,39)} = 22.08$, $p < 0.0001$) and treatment ($F_{(2,39)} = 5.018$, $p = 0.031$). As expected, the volume of the
310 RVNT increased across time, with E10 embryos having significantly larger RVNTs compared to both
311 E9.25 ($p < 0.0001$) and E9.5 ($p = 0.0002$), demonstrating the exceptional growth of the neural tube over
312 this period. There was a trend towards the RVNT of E9.5 embryos being larger than E9.25 ($p = 0.065$),
313 however this relationship was not statistically significant. Importantly, RVNT volume was significantly
314 smaller in NAE compared to vehicle-treated embryos ($0.197 \pm 0.01 \text{ mm}^3$ vs. $0.3224 \pm 0.04 \text{ mm}^3$) on E9.5
315 ($p = 0.0085$) and tended to be smaller on E10 as well, though this difference did not reach statistical
316 significance ($p = 0.1$). The thickness of the RVNT cell layer was also assessed, however while the cell
317 layer did grow thicker across time ($F_{(2,39)} = 9.142$, $p = 0.0006$), there was no significant effect of
318 treatment (Fig 1C). E10 embryos had increased widths compared to both E9.25 ($p = 0.0049$) and E9.5
319 ($p = 0.0012$). The increase in cell layer width corresponds to the larger overall volume at E10. The rapid
320 changes in RVNT volume across the first 24 hr post-alcohol exposure indicate that significant structural
321 changes are taking place and encourages further investigation into all factors by which alcohol could
322 affect growth, including alterations to cell proliferation. Additionally, while NAE-induced
323 dysmorphologies are evident later in development (11-14), no overt gross anatomical differences were
324 observed between vehicle and NAE-treated embryos at E9.5 (S2 Fig). Thus, alcohol-related changes in
325 tissue volume and shape are likely subtle at this time point and region- and timing-specific. Even

326 though the volumetric changes induced by NAE were transient, a brief period of growth inhibition within
327 this region of the neural tube during such an important and dynamic period of early development could
328 have long-lasting consequences on face and brain structure.

329 **NAE alters expression of key cilia-related genes, but not cilia** 330 **density in the RVNT**

331 Shh transduction occurs within the axoneme of primary cilia, nearly ubiquitous structures of
332 mammalian cells that play a particularly important role during embryonic development. Dysregulation of
333 RVNT primary cilia poses a risk to the normal development of brain regions that arise from this area of
334 the neural tube, namely midline structures such as the hypothalamus, septum, pituitary, and preoptic
335 area (45), many of which have been shown to be altered by NAE. Additionally, midline anomalies such
336 as hypertelorism are a hallmark of genetic ciliopathies and have also been reported in a subset of
337 patients with heavy prenatal alcohol exposure (4), suggesting an overlapping etiology between
338 ciliopathies and prenatal alcohol.

339 Based on the reduction in *Shh* and downstream cell cycle gene expression, we hypothesized
340 that we might find a coinciding NAE-induced change in either 1) the number of primary cilia or 2) cilia-
341 related genes in the RVNT. First, we examined the direct impact of NAE on primary cilia in the RVNT
342 by analyzing cilia density. Primary cilia were labeled for the cilia-specific small GTPase Arl13b at 6, 12,
343 or 24 hr following NAE (Fig 3A) and the number of cilia within the known volume of the RVNT were
344 analyzed using 3D image stacks from confocal images. A significant time (hours post-exposure) x
345 treatment interaction was found ($F_{(2,39)} = 3.642$, $p = 0.036$), as well as a main effect of time ($F_{(2,39)} =$
346 18.93 , $p < 0.0001$) (Fig 3B). No main effect of treatment was observed. No significant differences were
347 seen between vehicle and NAE embryos at any time point, though there was a trend towards an
348 increase in cilia density at the E9.5 (12 hr post-exposure) time point ($p = 0.087$). The density of cilia in
349 the RVNT significantly decreased over time, as there was a higher density of cilia at E9.25 compared to
350 both E9.5 and E10 ($p < 0.0001$ for both time points). This reduction in density is likely due to the

351 substantial growth of the neural tube during neurulation (Fig 2B-C), however the lack of a treatment
352 effect precludes alcohol-induced effects on cilia number as the mechanism of action of reduced cell
353 cycle gene expression.

354 **Fig 3. NAE alters expression of cilia-related genes in the RVNT but does not alter cilia density.**

355 A) Primary cilia in the RVNT were labeled with an anti-Arl13b antibody and stacks were compressed to
356 visualize cilia throughout the depth of the tissue in a single image. Cilia in the images are pseudo-
357 colored, scale bar = 10 μ m. B) Cilia density did not differ at any of the time points, but did decrease
358 across time points, as E9.5 and E10 had lower cilia density compared to E9.25 (n = 6-9). ** = $p < 0.01$,
359 **** = $p < 0.0001$, all values are expressed as mean + SEM. All gene expression data are the log₂ fold
360 change compared to the vehicle group (expressed as 0 on the graph) \pm SEM. C) NAE resulted in
361 significant changes to expression levels of genes related to ciliogenesis and post-transcriptional
362 modifications to ciliary tubulin, as well as genes implicated in genetic ciliopathies 6 hr after exposure. At
363 12 hr post-exposure, all genes had returned to baseline expression levels except for *Dpcc1*, which
364 remained significantly downregulated. E10 expression was not evaluated based on the return to
365 baseline observed for almost all genes at E9.5. Encoded proteins associated with these genes can be
366 found in Table 2. For all genes, n = 6-8 embryos per group. * = $p < 0.05$, ** = $p < 0.01$. Data are
367 expressed as log₂ fold change compared to the vehicle group (expressed as 0 on the graph) \pm SEM.

368 We further investigated primary cilia homeostasis and stability in the RVNT through analysis of
369 six cilia-related genes 6 or 12 hr following NAE: *Hap1*, *Rilpl2*, *Cep41*, *Nek4*, *Evc*, and *Dpcc1*. These time
370 points were focused on since almost all genes returned to baseline expression after 12 hr (Table 2, Fig
371 3C). These genes were chosen due to their known roles in important ciliary processes including
372 ciliogenesis, ciliary protein trafficking, or cilia stability through maintenance of post-translational
373 modification and/or genes that have mutations associated with human genetic ciliopathies. Based on
374 our *a priori* hypothesis that cilia-related genes would be most affected at the 6 hr time point (E9.25),
375 each time point was analyzed separately. At E9.25, NAE upregulated two of the genes, *Hap1* and
376 *Rilpl2* (1.19 and 0.37 log₂ fold change, respectively), in the RVNT (Table 2; Fig 3C). However,

377 expression levels of these genes returned to baseline by E9.5 (Table 2, Fig 3C). The other four genes
 378 (*Cep41*, *Nek4*, *Evc*, and *Dpcd*) showed marked downregulation 6 hr following NAE (E9.25) (Table 2,
 379 Fig 3C). *Dpcd* remained significantly downregulated (-0.467 log₂ fold change; Table 2, Fig 3C) 12 hr
 380 after NAE; however, expression of *Cep41*, *Nek4*, and *Evc* had returned to control levels. These genes
 381 have prominent roles related to cilia function, stability, and ciliogenesis. The NAE-induced dysregulation
 382 of these genes precedes and coincides with the downregulation of important morphogenic and cell
 383 proliferation pathways as well as reductions in RVNT volume.

384 **Table 2. Statistical results for cilia-related genes.**

Gene	Associated protein	Function	Log ₂ Fold Change	t(df)	Raw p-value
<i>Hap1</i>	Huntingtin-associated Protein 1	Ciliogenesis	E9.25: 1.19 E9.5: 0.448	3.364(10) 1.034(16)	0.0072* 0.3166
<i>Rilpl2</i>	Rab-Interacting Lysosomal Protein-Like 2	Ciliogenesis, protein trafficking	E9.25: 0.37 E9.5: -0.039	2.567(10) 0.238(18)	0.0281* 0.814
<i>Cep41</i>	Centrosomal Protein 41	Post-translational modifications of ciliary tubulin	E9.25: -1.61 E9.5: -0.179	3.675(13) 0.688(17)	0.0057* 0.501
<i>Nek4</i>	NIMA Related Kinase 4	Cell cycle, cilia function	E9.25: -0.45 E9.5: -0.048	2.361(14) 0.236(18)	0.033* 0.816
<i>Dpcd</i>	Deleted In Primary Ciliary Dyskinesia Homolog (mouse)	Generation and maintenance of ciliated cells	E9.25: -0.40 E9.5: -0.467	2.711(13) 2.389(19)	0.0178* 0.0274*
<i>Evc</i>	Ellis-van Creveld syndrome protein homolog (mouse)	Localized to cilia, interacts with Smo, Gli trafficking	E9.25: -0.43 E9.5: -0.175	2.548(14) 0.565(15)	0.0232* 0.5801

* = Remain significant following correction for multiple comparisons.

385

386

387 **Partial knockdown of cilia gene *Kif3a* interacts with NAE to affect** 388 **adolescent behavior**

389 To further test the hypothesis that disruption of normal cilia function is a mechanism for the
390 consequences of NAE, we utilized a transgenic mouse strain with a partial deletion of *Kif3a*, a gene that
391 codes for an intraflagellar transport protein. Full deletion of *Kif3a*, is a well-characterized ciliopathy
392 model (24, 26, 46, 47), and if NAE interacts with cilia function, then *Kif3a* heterozygosity would both
393 phenocopy and exacerbate NAE. We focused on a NAE effect that we have previously shown to be
394 robust and reproducible, behavioral change during adolescence (11). Adolescent male and female mice
395 exposed to E9.0 alcohol were tested on a battery of behavioral tasks, but since the largest behavioral
396 changes occurred in males, we discuss behavior from male, rather than female, mice in detail (for
397 female data refer to Fig S3B, S4A-D; S1 Table). Sex-specific effects of early gestational alcohol have
398 been previously reported to emerge in adolescence and adulthood and likely result from postnatal sex
399 differences, as opposed to embryonic effects of alcohol

400 We first examined motor coordination, using an accelerating rotarod performance across five
401 repeated trials. Although rotarod performance for all mice improved from the first to the fifth trial ($F_{(4,192)}$
402 = 28.4, $p < 0.0001$), NAE persistently impaired motor coordination, as revealed by a main effect of
403 NAE, regardless of *Kif3a* genotype ($F_{(1,48)} = 5.1$; $p = 0.028$; Fig S3). Previous research has suggested
404 that the etiology of cerebellar deficits caused by mid-stage NAE is likely alcohol-induced apoptosis in
405 the rostral rhombic lip, from which the cerebellum arises (5). The lack of an NAE x genotype interaction
406 indicates that primary cilia are not critical for these motor incoordination effects. While it is possible that
407 alcohol earlier or later in development could have more direct effects on primary cilia-mediated
408 mechanisms in the cerebellum, the middle of neurulation appears to be a critically sensitive period for
409 cerebellar defects, as our previous research has suggested that alcohol administered on E7 (O'Leary-
410 Moore & Sulik, *unpublished observations*) or E8 (11) has a less pronounced impact on motor
411 coordination.

412 However, when we examined elevated plus maze (EPM) exploration, a two-way ANOVA found
413 a significant genotype x treatment interaction ($F_{(1,49)} = 6.9$; $p = 0.01$) on total arm entries. Vehicle-treated
414 *Kif3a^{+/-}* and NAE *Kif3a^{+/+}* mice were more active than were vehicle-treated *Kif3a^{+/+}* mice ($p = 0.006$ and
415 $p = 0.04$, respectively) (Fig 4A), while NAE *Kif3a^{+/-}* had comparably high levels of activity but were not
416 statistically different from vehicle-treated *Kif3a^{+/+}* mice ($p = 0.061$). This result replicates our previous
417 findings on early NAE (11) and indicates that *Kif3a* heterozygosity phenocopies a locomotor
418 hyperactivity caused by NAE. Supporting the hypothesis that NAE and *Kif3a^{+/-}* also affect anxiety-like
419 behavior, there was a significant genotype x treatment interaction on the percentage of open arm time
420 ($F_{(1,49)} = 3.9$; $p = 0.05$) (Fig 4B), but not the percent of open arm entries (Fig 4C). *Post hoc* analysis
421 revealed that both vehicle-treated and NAE *Kif3a^{+/-}* mice spent a greater percentage of time on the
422 open arms than did the vehicle-treated *Kif3a^{+/+}* mice ($p < 0.001$ and $p = 0.01$, respectively). Although
423 NAE in *Kif3a^{+/+}* tended to phenocopy *Kif3a^{+/-}* on the open arm time, this effect was not significant in the
424 *post hoc* analyses. To test whether NAE alone affects open arm time in the *Kif3a^{+/+}* mice and confirm
425 our previous results using a two-sample *t*-test (11, 12), we ran this same statistical analysis ($t_{(20)} = 3.0$; p
426 $= 0.007$; Fig 4B) and found that that early NAE increases the percent of time on the open arms. Overall,
427 these results indicate that NAE and *Kif3a* heterozygosity phenocopy each other's effects on the EPM.
428 **Fig 4. Partial loss of cilia motor transport gene *Kif3a* phenocopies and potentiates the effect of**
429 **NAE on behavioral performance in adolescent male mice.** A) Vehicle-treated *Kif3a^{+/-}* and NAE WT
430 mice made more arm entries on the EPM than did vehicle-treated WT mice. B) Vehicle-treated and
431 NAE *Kif3a^{+/-}* mice spent a greater percentage of time on the open arms vs. vehicle-treated WT mice. C)
432 Percent of entries into the open arms was not significantly affected by genotype or treatment. D-F)
433 Significant ($p < 0.05$) *post hocs* are shown as letters on each graph. a: vs. vehicle-treated WT, b: vs.
434 vehicle-treated *Kif3a^{+/-}*, c: vs. NAE WT. D) NAE *Kif3a^{+/-}* mice were more active than vehicle-treated WT
435 mice during all time bins and were more active than NAE WT mice during the 2nd and 4th bins and more
436 active than vehicle-treated *Kif3a^{+/-}* mice during the final bin. Bracket = genotype x treatment interaction.
437 NAE *Kif3a^{+/-}* mice had more total beam breaks compared to the NAE WT and vehicle *Kif3a^{+/-}* mice. E)

438 NAE mice traveled further in the center of the open field compared to vehicle-treated mice. In addition,
439 NAE *Kif3a*^{+/-} mice traveled further than NAE WT or vehicle *Kif3a*^{+/-} groups. Bracket = main effect of
440 treatment. F) NAE animals spent more time in the center of the chamber compared to vehicle-treated
441 mice across time, and NAE *Kif3a*^{+/-} mice spending more time in the center compared to both NAE WT
442 and vehicle *Kif3a*^{+/-} mice. Bracket = main effect of treatment. For all groups, n's = 11-15 litters, with
443 same genotype littermates averaged into a single datum for each litter. For all graphs, * = $p < 0.05$, ** =
444 $p < 0.01$, *** = $p < 0.001$. All data are shown as group means + SEM.

445 Since the EPM is a relatively brief exposure to a complex novel environment and our procedure
446 did not assess habituation to the maze, we further measured exploratory behavior and activity in an
447 open field test across a 1-hr period. A three-way mixed ANOVA revealed a significant genotype x
448 treatment x time bin interaction on overall horizontal activity ($F_{(3,141)} = 4.3$; $p = 0.006$) (Fig 4D). *Post hoc*
449 analysis revealed that NAE *Kif3a*^{+/-} mice were more active than vehicle-treated *Kif3a*^{+/+} mice during
450 each of the 15-min time bins ($p = 0.002, 0.001, 0.032, \text{ and } 0.046$, respectively), and were more active
451 than NAE *Kif3a*^{+/+} mice during the 2nd and the final 15-min time bins ($p = 0.018 \text{ and } 0.006$, respectively).
452 NAE *Kif3a*^{+/-} mice were also more active than vehicle-treated *Kif3a*^{+/-} mice during the final 15-min time
453 bin ($p = 0.013$). Since the persistently high activity of the NAE *Kif3a*^{+/-} mice suggests impaired
454 habituation, we calculated a habituation index, expressing data from each 15-min time bin as a
455 percentage of the initial time bin (i.e. min 0-15). A significant 3-way interaction (genotype x treatment x
456 time bin; $F_{(3,141)} = 2.0$; $p = 0.039$) revealed that while all groups reduced their activity over the hour, in
457 the final time bin, NAE *Kif3a*^{+/-} mice were significantly less habituated than were the vehicle-treated
458 *Kif3a*^{+/-} mice and the NAE *Kif3a*^{+/+} mice ($p = 0.02 \text{ and } 0.03$, respectively). These groups had an initial
459 bout of heightened activity, relative to the vehicle-treated *Kif3a*^{+/+} mice, but NAE *Kif3a*^{+/-} mice
460 maintained a higher level of activity throughout the test.

461 There were significant main effects of NAE on several specific measures of activity, including
462 repeated beam breaks ($F_{(1,47)} = 4.1$; $p = 0.05$, S2 Table), center distance ($F_{(1,47)} = 9.4$; $p = 0.004$, Fig
463 4E), and center time ($F_{(1,47)} = 12.5$; $p = 0.001$, Fig 4F). *Kif3a*^{+/-} genotype also had significant effects

464 upon repeated beam breaks ($F_{(1,47)} = 5.2$; $p = 0.03$, S2 Table), center distance ($F_{(1,47)} = 10.6$; $p = 0.002$,
465 Fig 4E), and center time ($F_{(1,47)} = 7.4$; $p = 0.009$, Fig 4F) Both NAE and *Kif3a*^{+/-} genotype significantly
466 affected the number of rears, rotations, and total distance (statistics shown in S2 Table). On each of
467 these measures, NAE *Kif3a*^{+/-} mice were the most active treatment group indicating an additive effect of
468 *Kif3a* genotype and NAE.

469 To further illustrate the heightened activity of the NAE *Kif3a*^{+/-} mice relative to the other groups,
470 as predicted by our hypothesis, we analyzed overall horizontal activity (Fig 4D), center distance (Fig
471 4E), and center time (Fig 4F) as 60-min totals and used Bonferroni *post hoc* tests to compare NAE
472 *Kif3a*^{+/-} to NAE *Kif3a*^{+/+} mice (effect of genotype within NAE mice) or vehicle *Kif3a*^{+/-} mice (effect of NAE
473 within the heterozygotes), vehicle *Kif3a*^{+/-} to vehicle *Kif3a*^{+/+} (effect of genotype alone), and NAE *Kif3a*^{+/-}
474 to vehicle *Kif3a*^{+/+} mice (effect of NAE within the wild-types). The NAE *Kif3a*^{+/-} mice were more active
475 than their NAE *Kif3a*^{+/+} littermates ($p = 0.001$ for horizontal activity, 0.002 for center distance, and 0.006
476 for center time), and the vehicle *Kif3a*^{+/-} mice ($p = 0.003$ for horizontal activity, 0.015 for center distance,
477 and 0.003 for center time). There were no significant effects of NAE or *Kif3a*^{+/-} alone. The heightened
478 overall activity levels, as well as activity specific to the center of the open field which may reflect altered
479 anxiety-like behavior, confirm our prior results from early NAE that open field activity is a sensitive index
480 for the effects of early gestational alcohol exposure (11, 12). The greater sensitivity of the *Kif3a*^{+/-} in the
481 open field versus the EPM is likely due to differences in the test duration because the differences
482 between treatment and genotype groups appear to become greater as exploration patterns adapt to the
483 environment.

484 Brain width and ventricle area were also analyzed in a subset of adolescent male mice (n = 4-5
485 per group) chosen based on performance closest to the group means on open field horizontal activity.
486 Neither genotype nor prenatal treatment significantly affected ventricle area, though *Kif3a*^{+/-} mice
487 tended to have larger ventricles ($F_{(1,13)} = 3.767$, $p = 0.0743$; Fig S5A). A genotype-treatment interaction
488 was found for midline brain width ($F_{(1,13)} = 9.206$, $p = 0.0096$; Fig S5B), as well as a main effect of
489 treatment ($F_{(1,13)} = 27.55$, $p = 0.0002$). Dunnett's multiple comparison test was used to compare each

490 group to vehicle-treated *Kif3a*^{+/+} animals, and it was determined that the brains in all three other groups
491 were narrower (vs. *Kif3a*^{+/+} NAE: $p = 0.0001$; vs. *Kif3a*^{+/-} Veh: $p = 0.0308$; vs. *Kif3a*^{+/-} NAE: $p = 0.0018$).
492 In addition, a main effect of genotype was found for medial brain height, with *Kif3a*^{+/-} mice having
493 shorter medial height compared to *Kif3a*^{+/+} mice ($F_{(1,13)} = 6.332$, $p = 0.0258$; Fig S5C). Thus, the partial
494 deletion of *Kif3a* resulted in smaller brains in adolescence that coincided with behavioral abnormalities.

495 Discussion

496 The studies described here demonstrate that NAE disrupts the Shh pathway and cell cycle gene
497 expression, and causes a reduction in RVNT volume during the first 24 hr following exposure. In
498 addition, NAE disrupts expression of genes related to ciliogenesis and protein trafficking (Fig 4). Finally,
499 cilia gene-alcohol interactions were further demonstrated through the use of *Kif3a* transgenic mice, a
500 model of genetic ciliopathies (46). NAE male *Kif3a*^{+/-} exhibited exacerbated behavioral impairments on
501 the open field and EPM compared to controls and WT NAE mice, implicating cilia in specific behavioral
502 deficits. The current results support that early gestational alcohol exposure disrupts the Shh pathway,
503 either independently or as a consequence of primary cilia dysregulation. Future work will focus on the
504 exact impact of prenatal alcohol on primary cilia function and whether cilia dysfunction in the RVNT
505 causes the observed downregulation of the Shh pathway and if impaired cilia function contributes to the
506 development of craniofacial and midline CNS defects following prenatal alcohol exposure (11-14).
507 Additionally, these data have implications beyond the embryonic period and the neural tube, including
508 informing the emerging study of enhanced cancer risk in human alcoholics. Dysregulation of the
509 developmental signaling pathways, such as Shh, contribute to cancer pathogenesis (48) and more
510 research is focusing on primary cilia dysfunction as a mediating factor in cancer development (49).

511

512 **NAE disrupts the Shh pathway and cilia function in the neural** 513 **tube**

514 These studies confirm that NAE downregulated Shh pathway expression, similar to other FASD
515 models targeting early points of gestation (6-10). We observed decreased *Shh* and *Gli1* expression in
516 the RVNT of NAE embryos during the first 24 hr post-exposure. These reductions coincided with
517 increased levels of the Gli3^{Rep} form 12 hr following NAE. These data are the first to report altered Shh
518 signaling following alcohol exposure during neurulation. While *Gli2* gene expression was not affected
519 by NAE at either time point, it is possible that the ratio of the different forms of Gli2 was altered by NAE
520 while not impacting levels of mRNA, similar to what was found for Gli3. Like Gli3, Gli2 is found in full-
521 length activator and cleaved repressor forms, though studies have suggested that Gli2 acts primarily as
522 a transcriptional activator in the mouse neural tube (50-52), meaning the majority of Gli2 will be found in
523 the full-length form. However, currently available antibodies cannot reliably identify the various forms of
524 Gli2, in part due to the dearth of antibodies that bind to the correct epitope of the protein to allow for
525 detection of the cleaved repressor (N-terminus). It will be possible to address this question once
526 validated antibodies targeting different amino acid sequences of mouse Gli2 become available.

527 The molecular mechanisms of action of alcohol on the Shh pathway remain unclear. Alcohol
528 could act directly on the Shh pathway through interference with upstream regulator proteins, such as
529 Hoxd's (53), Sox2/3 (54), or Hand2 (best described in the embryonic limb bud) (55), or the Shh co-
530 receptor Cdon (56), disruption of cholesterol (57) or other proteins necessary for Shh modulation, or
531 activation of pathway inhibitors such as PKA (8) or Tbx2 (58). Our data suggest that alcohol could
532 indirectly disrupt the Shh pathway as a downstream consequence of the observed dysregulation of
533 primary cilia genes and their related functions. Downregulation of Gli proteins can cause a negative
534 feedback loop in Shh expression as the Gli proteins target multiple members of the Shh path, including
535 Ptc (59). The possibility that alcohol initiates a negative feedback loop of the Shh pathway is supported
536 by the concomitant reduction in expression of pro-proliferative genes known to be downstream of Gli's,

537 *Ccnd1*, *Ccnd2*, and *Fgf15*. Expression of other targets of Gli-mediated transcription may have been
538 impacted as well. The unique expression profiles of these genes during the 24 hr post-NAE indicate
539 possible differences between these molecules in alcohol sensitivity or presence of compensatory
540 mechanisms in the neural tube. The impact of reduced pro-proliferative genes was observed as a
541 smaller RVNT volume at E9.5. Since previous work from our laboratory has shown little to no excessive
542 apoptosis in the rostral basal or floor plates of the neural tube following E9.0 alcohol exposure (5), the
543 most likely explanation for the reduced RVNT volume is decreased cell proliferation. The lack of
544 increased apoptosis in the rostroventral portion of the neural tube following NAE stands in stark
545 contrast to the pronounced apoptosis throughout the neuroectoderm following exposure at earlier time
546 points and suggests region- and timing-specific mechanisms of alcohol-induced tissue damage. While
547 not quantitatively measured in this study, the RVNT's of NAE embryos displayed some shape
548 differences compared to controls, as can be seen in Fig 2. Since neural patterning is a primary function
549 of Shh, altered cell migration in the RVNT could be another consequence of disrupted Shh signaling. It
550 is also possible that reduced activation of the Shh pathway in the ventral neural tube allows for
551 redistribution of morphogens and increased expression of Wnt within the dorsal neural tube. Since the
552 dorsal neural tube also contributes to craniofacial development through Wnt and Bmp signaling, an
553 imbalance in the morphogenic gradients would likely result in abnormal growth trajectories of regions
554 arising from these portions of the neural tube.

555 The Shh pathway requires properly functioning primary cilia and our data demonstrating NAE-
556 induced disruptions to cilia gene expression support that NAE impairs primary cilia function. While cilia
557 density was not affected in the current study, NAE resulted in changes to cilia-related genes in the
558 RVNT that emerge within the first 6 hr following alcohol exposure and extend to the Gli family of
559 transcription factors after 6-12 hr. These data demonstrate that NAE rapidly dysregulates primary cilia
560 gene expression and identifies ciliogenesis, protein trafficking, and maintenance of cilia stability as
561 targets of NAE. At E9.25, NAE upregulated *Hap1* and *Rilpl2* in the RVNT (Table 2; Fig 3C), two genes
562 associated with ciliogenesis (60, 61). *Hap1* is named for its role in Huntington's disease (60) and has

563 been shown to mediate ciliogenesis through interaction with the Huntingtin protein (Htt). While little is
564 known regarding ciliopathies in patients with Huntington's disease, patients with Huntington's, and mice
565 with introduction of mutated Htt, exhibit abnormally increased cilia number and length (60, 62).
566 Furthermore, mutated Htt disrupts the normal binding of Hap1 to dynein, affecting protein transport
567 (63). In addition to its role in ciliogenesis, *Rilpl2* is involved in ciliary protein transport (61). Increased
568 expression of ciliogenesis-related genes could be a result of alcohol-induced disruptions of normal cell
569 cycle progression in the RVNT, as cilia are retracted and extended during mitosis.

570 In contrast, *Cep41*, *Nek4*, *Evc*, and *Dpcd* were downregulated in NAE embryos at E9.25 (Table
571 2, Fig 3C). *Cep41* is known to be mutated in patients with the genetic ciliopathy Joubert syndrome
572 (64). Patients with Joubert syndrome display many symptoms similar to other ciliopathies, including
573 renal, ocular, digital, and neurological abnormalities. Notably, patients with Joubert syndrome also
574 show clinical symptoms that overlap with some features of FASD, including cerebellar dysplasia,
575 impaired motor function, abnormal eye development, polydactyly, and craniofacial dysmorphologies. In
576 mouse and zebrafish models, loss of *Cep41* causes ciliopathy-like phenotypes, including brain
577 malformations (64). Thus, even transient downregulation of this gene could impact normal CNS
578 development. In addition, *Cep41* is implicated in polyglutamylation of ciliary α -tubulin; loss of tubulin
579 glutamylation could result in structural instability and affect ciliary assembly and transport. Further
580 studies are needed to determine if changes to *Cep41* expression are directly linked to glutamylation
581 status of ciliary tubulin in the RVNT following NAE. *Nek4* has a role in mediating ciliary assembly and
582 integrity, possibly through *Nek4*'s regulation of microtubules (65). The gene *Dpcd* is associated with
583 another ciliopathy, Primary Ciliary Dyskinesia, caused by dysfunction of motile cilia in the respiratory
584 tract and reproductive systems, resulting in respiratory difficulties and infertility (66). *Dpcd* has been
585 implicated in the formation and maintenance of cilia and is upregulated during cell division. Finally,
586 downregulation of *Evc* could have direct impact on trafficking of the Shh pathway proteins Smo and the
587 Gli family (67, 68). Ellis-van Creveld syndrome, caused by a mutation in *Evc*, is a genetic ciliopathy
588 presenting with polydactyly and other digital anomalies, congenital heart defects, and other skeletal

589 abnormalities. Similar skeletal malformations have been noted in humans and rodent models of FASD
590 (69-71). The decrease in *Cep41* was particularly interesting, as polyglutamylation of tubulin is important
591 for protein trafficking within the cilia, including Shh pathway proteins (72). In addition, *Evc* is known to
592 play a role in Gli protein trafficking (67). Together, the downregulation of these two genes suggests
593 disruption of Gli signaling within the cilia as a likely mechanism for the later reduction in *Ccnd1*
594 expression. The observed downregulation of *Dpcd*, a gene normally upregulated during cilia formation
595 and cell division (66), further supports the conclusion that the cell cycle has been affected by NAE as
596 early as 6 hr post-exposure. Transient changes in cell proliferation in this region of the neural tube
597 would impact the development of midline brain and craniofacial tissue (4, 11, 13, 14). A schematic of
598 cilia genes altered following NAE at 6 and 12 hr is shown in Fig 5.

599 **Fig 5. Schematic of a primary cilium.** This representation of the primary cilium includes the axoneme,
600 basal body, and centriole and displays differentially expressed genes related to cilia
601 structure/ciliogenesis/protein trafficking 6 hr post-exposure and the Shh pathway and cilia function 6-24
602 hr post-exposure. Orange outlines indicate upregulated genes whereas blue outlines denote genes that
603 were downregulated by NAE.

604 **NAE interacts with cilia gene knockdown to alter exploratory** 605 **behavior during adolescence**

606 Mice lacking one copy of the *Kif3a* gene were used to demonstrate that prenatal alcohol
607 interacts with cilia function. The *Kif3a* mutant mouse is a well-characterized model of genetic ciliopathy
608 (24, 46, 73) as *Kif3a* mutant mice phenocopy many human ciliopathies, including hypertelorism, facial
609 clefting, and brain abnormalities (46, 74). Similar to the defects seen in conditional *Kif3a* mutant mice,
610 NAE mice can exhibit abnormal cortical hemispheres and ventral midline brain structures (13, 14) and
611 hypertelorism has been reported in some patients with heavy prenatal alcohol exposure who lack the
612 classic FAS facial features (4, 75). *Kif3a* heterozygous mice have been shown to display similar
613 physical abnormalities, such as situs inversus, to the full knockout but at a much lower rate (76), as

614 *Kif3a*^{-/-} die by E10. *Kif3a*^{+/-} mice also have reported reduced *Kif3a* gene expression in the bone and
615 osteoblasts at 6 weeks old (77). These mice also display abnormal *Gli2* expression (77), supporting
616 that *Kif3a* interacts with Shh signaling and that *Kif3a*^{+/-} mice have abnormal cilia function, as *Gli2*
617 processing is a critical function of primary cilia during development. In the current study, exploratory
618 behavior in two novel environments (EPM and open field), which relies heavily on the cortico-limbic and
619 hypothalamic circuitry derived from the RVNT, was sensitive to both NAE and *Kif3a* genotype effects,
620 as well as NAE-genotype interactions. NAE and *Kif3a*^{+/-} similarly heightened exploration of the EPM
621 open arms and the center of the open field and increased total activity on the EPM and in the open
622 field. Increased exploratory behavior suggests an impaired stress and or anxiety-related response, as
623 previously observed following gestational alcohol exposure (35). While the current evidence cannot
624 definitively show that the perturbed behaviors observed in NAE and *Kif3a*^{+/-} mice are due to a common
625 mechanism, the persistence of hyperactivity and impaired open field habituation observed in the NAE
626 *Kif3a*^{+/-} mice lends support to the hypothesis that variants of a key primary cilia gene might act as a risk
627 factor for certain behavioral effects of NAE.

628 **Conclusions**

629 In conclusion, these data demonstrate that neurulation-stage alcohol exposure decreases Shh
630 pathway signaling, Shh-mediated cell cycle gene expression, and alters expression of genes related to
631 ciliogenesis and protein trafficking in a region of the neural tube that gives rise to alcohol-sensitive
632 ventral midline brain structures. These results are the first to suggest primary cilia dysfunction as a
633 possible pathogenic mechanism of prenatal alcohol exposure, either through downstream effects on the
634 Shh pathway or other mechanisms that remain to be elucidated. Furthermore, NAE interacts with
635 primary cilia to alter open field and EPM behavior in *Kif3a* mutant male mice during adolescence.
636 Together, these data demonstrate an interaction of prenatal alcohol and primary cilia, possibly resulting
637 in an alcohol-induced “transient ciliopathy” and contributing to midline craniofacial and CNS defects in
638 FASD.

639 **Acknowledgements**

640 We thank Jamie Leitzinger, Divya Venkatasubramanian, Haley Mendoza-Romero, Laura
641 Murdaugh, and Debbie Dehart for their technical assistance on this project.

642

643 **Competing interests**

644 The authors have no conflicts of interest to report.

645

646 **Funding**

647 Funding to support this research was provided by the National Institutes of Health/National
648 Institute of Alcohol and Alcoholism [U01AA021651 and R01AA026068 to SEP, F32AA026479 to KEB]
649 and conducted as part of the Collaborative Initiative on Fetal Alcohol Spectrum Disorders (CIFASD).

650

651 **Author Contributions**

652 Conceptualization: KEB, EWF, and SEP

653 Methodology: KEB, EWF, and SEP

654 Investigation: KEB and EWF

655 Formal Analysis: KEB and EWF

656 Visualization: KEB and EWF

657 Writing – Original Draft Preparation: KEB and EWF

658 Writing – Review & Editing: KEB, EWF, and SEP

659

References

- 660 1. May PA, Chambers CD, Kalberg WO, Zellner J, Feldman H, Buckley D, et al. Prevalence of
661 fetal alcohol spectrum disorders in 4 US communities. *JAMA*. 2018;319(5):474-82.
- 662 2. Cook CS, Nowotny AZ, Sulik KK. Fetal alcohol syndrome: eye malformations in a mouse model.
663 *Archives of Ophthalmology*. 1987;105(11):1576-81.
- 664 3. Godin EA, O'Leary-Moore SK, Khan AA, Parnell SE, Ament JJ, Dehart DB, et al. Magnetic
665 Resonance Microscopy Defines Ethanol-Induced Brain Abnormalities in Prenatal Mice: Effects of Acute
666 Insult on Gestational Day 7. *Alcoholism: Clinical and Experimental Research*. 2010;34(1):98-111.
- 667 4. Suttie M, Wetherill L, Jacobson SW, Jacobson JL, Hoyme HE, Sowell ER, et al. Facial curvature
668 detects and explicates ethnic differences in effects of prenatal alcohol exposure. *Alcoholism: Clinical
669 and Experimental Research*. 2017.
- 670 5. Dunty WC, Chen Sy, Zucker RM, Dehart DB, Sulik KK. Selective Vulnerability of Embryonic Cell
671 Populations to Ethanol-Induced Apoptosis: Implications for Alcohol-Related Birth Defects and
672 Neurodevelopmental Disorder. *Alcoholism: Clinical and Experimental Research*. 2001;25(10):1523-35.
- 673 6. Kietzman HW, Everson JL, Sulik KK, Lipinski RJ. The teratogenic effects of prenatal ethanol
674 exposure are exacerbated by Sonic Hedgehog or GLI2 haploinsufficiency in the mouse. *PloS one*.
675 2014;9(2):e89448.
- 676 7. Smith SM, Garic A, Flentke GR, Berres ME. Neural crest development in fetal alcohol
677 syndrome. *Birth Defects Research Part C: Embryo Today: Reviews*. 2014;102(3):210-20.
- 678 8. Aoto K, Shikata Y, Higashiyama D, Shiota K, Motoyama J. Fetal ethanol exposure activates
679 protein kinase A and impairs Shh expression in prechordal mesendoderm cells in the pathogenesis of
680 holoprosencephaly. *Birth Defects Research Part A: Clinical and Molecular Teratology*. 2008;82(4):224-
681 31.
- 682 9. Zhang C, Frazier JM, Chen H, Liu Y, Lee JA, Cole GJ. Molecular and morphological changes in
683 zebrafish following transient ethanol exposure during defined developmental stages. *Neurotoxicol
684 Teratol*. 2014;44:70-80.
- 685 10. Higashiyama D, Saito H, Komada M, Takigawa T, Ishibashi M, Shiota K. Sequential
686 developmental changes in holoprosencephalic mouse embryos exposed to ethanol during the
687 gastrulation period. *Birth defects research Part A, Clinical and molecular teratology*. 2007;79(7):513-23.
- 688 11. Fish E, Holloway H, Rumble A, Baker L, Wieczorek L, Moy S, et al. Acute alcohol exposure
689 during neurulation: Behavioral and brain structural consequences in adolescent C57BL/6J mice.
690 *Behavioural brain research*. 2016;311:70-80.
- 691 12. Fish E, Wieczorek L, Rumble A, Suttie M, Moy S, Hammond P, et al. the enduring impact of
692 neurulation stage alcohol exposure: A combined behavioral and structural neuroimaging study in adult
693 male and female C57bl/6j mice. *Behavioural brain research*. 2018;338:173-84.
- 694 13. Parnell SE, Holloway HT, O'Leary-Moore SK, Dehart DB, Paniaqua B, Oguz I, et al. Magnetic
695 resonance microscopy-based analyses of the neuroanatomical effects of gestational day 9 ethanol
696 exposure in mice. *Neurotoxicology and teratology*. 2013;39:77-83.
- 697 14. Parnell SE, O'Leary-Moore SK, Godin EA, Dehart DB, Johnson BW, Allan Johnson G, et al.
698 Magnetic Resonance Microscopy Defines Ethanol-Induced Brain Abnormalities in Prenatal Mice:
699 Effects of Acute Insult on Gestational Day 8. *Alcoholism: Clinical and Experimental Research*.
700 2009;33(6):1001-11.
- 701 15. Cortés CR, Metzis V, Wicking C. Unmasking the ciliopathies: craniofacial defects and the
702 primary cilium. *Wiley Interdisciplinary Reviews: Developmental Biology*. 2015;4(6):637-53.
- 703 16. Gerdes JM, Davis EE, Katsanis N. The Vertebrate Primary Cilium in Development,
704 Homeostasis, and Disease. *Cell*. 2009;137(1):32-45.
- 705 17. Abdelhamed ZA, Wheway G, Szymanska K, Natarajan S, Toomes C, Inglehearn C, et al.
706 Variable expressivity of ciliopathy neurological phenotypes that encompass Meckel–Gruber syndrome

- 707 and Joubert syndrome is caused by complex de-regulated ciliogenesis, Shh and Wnt signalling defects.
708 Human molecular genetics. 2013;dds546.
- 709 18. Waters AM, Beales PL. Ciliopathies: an expanding disease spectrum. *Pediatric Nephrology*.
710 2011;26(7):1039-56.
- 711 19. Alby C, Piquand K, Huber C, Megarbané A, Ichkou A, Legendre M, et al. Mutations in KIAA0586
712 cause lethal ciliopathies ranging from a hydrolethalus phenotype to short-rib polydactyly syndrome. *The*
713 *American Journal of Human Genetics*. 2015;97(2):311-8.
- 714 20. Shaheen R, Shamseldin HE, Loucks CM, Seidahmed MZ, Ansari S, Khalil MI, et al. Mutations in
715 CSPP1, encoding a core centrosomal protein, cause a range of ciliopathy phenotypes in humans. *The*
716 *American Journal of Human Genetics*. 2014;94(1):73-9.
- 717 21. Cortellino S, Wang C, Wang B, Bassi MR, Caretti E, Champeval D, et al. Defective ciliogenesis,
718 embryonic lethality and severe impairment of the Sonic Hedgehog pathway caused by inactivation of
719 the mouse complex A intraflagellar transport gene *Ift122/Wdr10*, partially overlapping with the DNA
720 repair gene *Med1/Mbd4*. *Developmental biology*. 2009;325(1):225-37.
- 721 22. Stottmann R, Tran P, Turbe-Doan A, Beier DR. *Ttc21b* is required to restrict sonic hedgehog
722 activity in the developing mouse forebrain. *Developmental biology*. 2009;335(1):166-78.
- 723 23. Tran PV, Haycraft CJ, Besschetnova TY, Turbe-Doan A, Stottmann RW, Herron BJ, et al. *THM1*
724 negatively modulates mouse sonic hedgehog signal transduction and affects retrograde intraflagellar
725 transport in cilia. *Nature genetics*. 2008;40(4):403-10.
- 726 24. Brugmann S, Chang C-F, Millington G. *GLI*-dependent Etiology of Craniofacial Ciliopathies. *The*
727 *FASEB Journal*. 2015;29(1_supplement):86.2.
- 728 25. Chang C-F, Chang Y-T, Millington G, Brugmann SA. Craniofacial ciliopathies reveal specific
729 requirements for *GLI* proteins during development of the facial midline. *PLoS genetics*.
730 2016;12(11):e1006351.
- 731 26. Brugmann SA, Allen NC, James AW, Mekonnen Z, Madan E, Helms JA. A primary cilia-
732 dependent etiology for midline facial disorders. *Human molecular genetics*. 2010;19(8):1577-92.
- 733 27. O'Leary-Moore SK, Parnell SE, Godin EA, Dehart DB, Ament JJ, Khan AA, et al. Magnetic
734 resonance microscopy-based analyses of the brains of normal and ethanol-exposed fetal mice. *Birth*
735 *Defects Research Part A: Clinical and Molecular Teratology*. 2010;88(11):953-64.
- 736 28. Schindelin J, Arganda-Carreras I, Frise E, Kaynig V, Longair M, Pietzsch T, et al. Fiji: an open-
737 source platform for biological-image analysis. *Nature methods*. 2012;9(7):676-82.
- 738 29. Osborn J, Yu C, Gabriel K, Weinberg J. Fetal ethanol effects on benzodiazepine sensitivity
739 measured by behavior on the elevated plus-maze. *Pharmacology Biochemistry and Behavior*.
740 1998;60(3):625-33.
- 741 30. File SE. Factors controlling measures of anxiety and responses to novelty in the mouse.
742 *Behavioural brain research*. 2001;125(1-2):151-7.
- 743 31. Fish E, Wieczorek L, Parnell S. Neurobehavioral Consequences Of Early Gestational Binge-like
744 Alcohol Exposure: Age-related Alterations In Male And Female C57bu6j Mice. *Alcoholism: Clinical &*
745 *Experimental Research*. 2015;39:165A.
- 746 32. McDonald JH. *Handbook of biological statistics*: Sparky House Publishing Baltimore, MD; 2009.
- 747 33. Livak KJ, Schmittgen TD. Analysis of relative gene expression data using real-time quantitative
748 PCR and the 2- $\Delta\Delta$ CT method. *Methods (San Diego, Calif)*. 2001;25(4):402-8.
- 749 34. Holson R, Pearce B. Principles and pitfalls in the analysis of prenatal treatment effects in
750 multiparous species. *Neurotoxicology and teratology*. 1992;14(3):221-8.
- 751 35. Wieczorek L, Fish EW, O'Leary-Moore SK, Parnell SE, Sulik KK. Hypothalamic-pituitary-adrenal
752 axis and behavioral dysfunction following early binge-like prenatal alcohol exposure in mice. *Alcohol*.
753 2015;49(3):207-17.
- 754 36. Wilson SL, Wilson JP, Wang C, Wang B, McConnell SK. Primary cilia and *Gli3* activity regulate
755 cerebral cortical size. *Developmental neurobiology*. 2012;72(9):1196-212.
- 756 37. Bangs F, Anderson KV. Primary cilia and mammalian hedgehog signaling. *Cold Spring Harbor*
757 *perspectives in biology*. 2017;9(5):a028175.

- 758 38. Jia Y, Wang Y, Xie J. The Hedgehog pathway: role in cell differentiation, polarity and
759 proliferation. *Arch Toxicol.* 2015;89(2):179-91.
- 760 39. Sherr CJ, Roberts JM. CDK inhibitors: positive and negative regulators of G1-phase
761 progression. *Genes & development.* 1999;13(12):1501-12.
- 762 40. Kasper M, Schnidar H, Neill GW, Hanneder M, Klingler S, Blaas L, et al. Selective modulation of
763 Hedgehog/GLI target gene expression by epidermal growth factor signaling in human keratinocytes.
764 *Molecular and cellular biology.* 2006;26(16):6283-98.
- 765 41. Alvarez-Medina R, Le Dreau G, Ros M, Martí E. Hedgehog activation is required upstream of
766 Wnt signalling to control neural progenitor proliferation. *Development.* 2009;136(19):3301-9.
- 767 42. Ishibashi M, McMahon AP. A sonic hedgehog-dependent signaling relay regulates growth of
768 diencephalic and mesencephalic primordia in the early mouse embryo. *Development.*
769 2002;129(20):4807-19.
- 770 43. Saitsu H, Komada M, Suzuki M, Nakayama R, Motoyama J, Shiota K, et al. Expression of the
771 mouse *Fgf15* gene is directly initiated by Sonic hedgehog signaling in the diencephalon and midbrain.
772 *Developmental dynamics : an official publication of the American Association of Anatomists.*
773 2005;232(2):282-92.
- 774 44. Fischer T, Faus-Kessler T, Welzl G, Simeone A, Wurst W, Prakash N. *Fgf15*-mediated control
775 of neurogenic and proneural gene expression regulates dorsal midbrain neurogenesis. *Dev Biol.*
776 2011;350(2):496-510.
- 777 45. Watson C, Paxinos G, Puelles L. *The mouse nervous system*: Academic Press; 2012.
- 778 46. Liu B, Chen S, Johnson C, Helms J. A ciliopathy with hydrocephalus, isolated craniosynostosis,
779 hypertelorism, and clefting caused by deletion of *Kif3a*. *Reproductive Toxicology.* 2014;48:88-97.
- 780 47. Lehti MS, Kotaja N, Sironen A. *KIF3A* is essential for sperm tail formation and manchette
781 function. *Molecular and cellular endocrinology.* 2013;377(1):44-55.
- 782 48. Bailey JM, Singh PK, Hollingsworth MA. Cancer metastasis facilitated by developmental
783 pathways: Sonic hedgehog, Notch, and bone morphogenic proteins. *Journal of cellular biochemistry.*
784 2007;102(4):829-39.
- 785 49. Michaud EJ, Yoder BK. The primary cilium in cell signaling and cancer. *Cancer research.*
786 2006;66(13):6463-7.
- 787 50. Ding Q, Motoyama J, Gasca S, Mo R, Sasaki H, Rossant J, et al. Diminished Sonic hedgehog
788 signaling and lack of floor plate differentiation in *Gli2* mutant mice. *Development.* 1998;125(14):2533-
789 43.
- 790 51. Matisse MP, Epstein DJ, Park HL, Platt KA, Joyner AL. *Gli2* is required for induction of floor plate
791 and adjacent cells, but not most ventral neurons in the mouse central nervous system. *Development.*
792 1998;125(15):2759-70.
- 793 52. Park H, Bai C, Platt K, Matisse M, Beeghly A, Hui C, et al. Mouse *Gli1* mutants are viable but
794 have defects in SHH signaling in combination with a *Gli2* mutation. *Development.* 2000;127(8):1593-
795 605.
- 796 53. Chen Y, Knezevic V, Ervin V, Hutson R, Ward Y, Mackem S. Direct interaction with *Hoxd*
797 proteins reverses *Gli3*-repressor function to promote digit formation downstream of *Shh*. *Development.*
798 2004;131(10):2339-47.
- 799 54. Ferri A, Favaro R, Beccari L, Bertolini J, Mercurio S, Nieto-Lopez F, et al. *Sox2* is required for
800 embryonic development of the ventral telencephalon through the activation of the ventral determinants
801 *Nkx2.1* and *Shh*. *Development.* 2013;140(6):1250-61.
- 802 55. Galli A, Robay D, Osterwalder M, Bao X, Bénazet J-D, Tariq M, et al. Distinct roles of *Hand2* in
803 initiating polarity and posterior *Shh* expression during the onset of mouse limb bud development. *PLoS*
804 *genetics.* 2010;6(4):e1000901.
- 805 56. Hong M, Krauss RS. *Cdon* mutation and fetal ethanol exposure synergize to produce midline
806 signaling defects and holoprosencephaly spectrum disorders in mice. *PLoS genetics.*
807 2012;8(10):e1002999.

- 808 57. Li Y-X, Yang H-T, Zdanowicz M, Sicklick JK, Qi Y, Camp TJ, et al. Fetal alcohol exposure
809 impairs Hedgehog cholesterol modification and signaling. *Laboratory investigation*. 2007;87(3):231.
- 810 58. Manning L, Ohyama K, Saeger B, Hatano O, Wilson SA, Logan M, et al. Regional
811 morphogenesis in the hypothalamus: a BMP-Tbx2 pathway coordinates fate and proliferation through
812 Shh downregulation. *Developmental cell*. 2006;11(6):873-85.
- 813 59. Shin SH, Kogerman P, Lindström E, Toftgård R, Biesecker LG. GLI3 mutations in human
814 disorders mimic *Drosophila cubitus interruptus* protein functions and localization. *Proceedings of the*
815 *National Academy of Sciences*. 1999;96(6):2880-4.
- 816 60. Keryer G, Pineda JR, Liot G, Kim J, Dietrich P, Benstaali C, et al. Ciliogenesis is regulated by a
817 huntingtin-HAP1-PCM1 pathway and is altered in Huntington disease. *The Journal of clinical*
818 *investigation*. 2011;121(11):4372-82.
- 819 61. Schaub JR, Stearns T. The Rilp-like proteins Rilpl1 and Rilpl2 regulate ciliary membrane
820 content. *Molecular biology of the cell*. 2013;24(4):453-64.
- 821 62. Liu J-P, Zeitlin SO. The long and the short of aberrant ciliogenesis in Huntington disease. *The*
822 *Journal of clinical investigation*. 2011;121(11).
- 823 63. Gauthier LR, Charrin BC, Borrell-Pages M, Dompierre JP, Rangone H, Cordelieres FP, et al.
824 Huntingtin controls neurotrophic support and survival of neurons by enhancing BDNF vesicular
825 transport along microtubules. *Cell*. 2004;118(1):127-38.
- 826 64. Lee JE, Silhavy JL, Zaki MS, Schroth J, Bielas SL, Marsh SE, et al. CEP41 is mutated in
827 Joubert syndrome and is required for tubulin glutamylation at the cilium. *Nature genetics*.
828 2012;44(2):193-9.
- 829 65. Coene KL, Mans DA, Boldt K, Gloeckner CJ, van Reeuwijk J, Bolat E, et al. The ciliopathy-
830 associated protein homologs RPGRIP1 and RPGRIP1L are linked to cilium integrity through interaction
831 with Nek4 serine/threonine kinase. *Hum Mol Genet*. 2011;20(18):3592-605.
- 832 66. Zariwala M, O'Neal WK, Noone PG, Leigh MW, Knowles MR, Ostrowski LE. Investigation of the
833 possible role of a novel gene, DPCD, in primary ciliary dyskinesia. *American journal of respiratory cell*
834 *and molecular biology*. 2004;30(4):428-34.
- 835 67. Caparrós-Martín JA, Valencia M, Reytor E, Pacheco M, Fernandez M, Perez-Aytes A, et al. The
836 ciliary Evc/Evc2 complex interacts with Smo and controls Hedgehog pathway activity in chondrocytes
837 by regulating Sufu/Gli3 dissociation and Gli3 trafficking in primary cilia. *Human molecular genetics*.
838 2012;22(1):124-39.
- 839 68. Dorn KV, Hughes CE, Rohatgi R. A Smoothed-Evc2 complex transduces the Hedgehog
840 signal at primary cilia. *Developmental cell*. 2012;23(4):823-35.
- 841 69. Kotch L, Dehart D, Alles A, Chernoff N, Sulik K. Pathogenesis of ethanol-induced limb reduction
842 defects in mice. *Teratology*. 1992;46(4):323-32.
- 843 70. McMechan AP, O'Leary-Moore SK, Morrison SD, Hannigan JH. Effects of prenatal alcohol
844 exposure on forepaw digit length and digit ratios in rats. *Developmental psychobiology*. 2004;45(4):251-
845 8.
- 846 71. Jones K, Smith D. Recognition of the fetal alcohol syndrome in early infancy. *The Lancet*.
847 1973;302(7836):999-1001.
- 848 72. Hong S-R, Wang C-L, Huang Y-S, Chang Y-C, Chang Y-C, Pusapati GV, et al. Spatiotemporal
849 manipulation of ciliary glutamylation reveals its roles in intraciliary trafficking and Hedgehog signaling.
850 *Nature communications*. 2018;9.
- 851 73. Takeda S, Yonekawa Y, Tanaka Y, Okada Y, Nonaka S, Hirokawa N. Left-right asymmetry and
852 kinesin superfamily protein KIF3A: new insights in determination of laterality and mesoderm induction
853 by kif3A^{-/-} mice analysis. *The Journal of cell biology*. 1999;145(4):825-36.
- 854 74. Dafinger C, Liebau MC, Elsayed SM, Hellenbroich Y, Boltshauser E, Korenke GC, et al.
855 Mutations in KIF7 link Joubert syndrome with Sonic Hedgehog signaling and microtubule dynamics.
856 *The Journal of clinical investigation*. 2011;121(7):2662-7.

- 857 75. Astley SJ, Clarren SK. Measuring the facial phenotype of individuals with prenatal alcohol
858 exposure: correlations with brain dysfunction. *Alcohol and alcoholism* (Oxford, Oxfordshire).
859 2001;36(2):147-59.
- 860 76. Marszalek JR, Ruiz-Lozano P, Roberts E, Chien KR, Goldstein LS. Situs inversus and
861 embryonic ciliary morphogenesis defects in mouse mutants lacking the KIF3A subunit of kinesin-II.
862 *Proceedings of the National Academy of Sciences*. 1999;96(9):5043-8.
- 863 77. Qiu N, Cao L, David V, Quarles LD, Xiao Z. Kif3a deficiency reverses the skeletal abnormalities
864 in Pkd1 deficient mice by restoring the balance between osteogenesis and adipogenesis. *PloS one*.
865 2010;5(12):e15240.
866

867 Supporting information

868 **S1 Fig. Uncropped western blot analysis of Gli3.** A) E9.25 (6 hr post-exposure) blot of Gli3 full
869 length (190 kDa), cleaved (83 kDa), and Gapdh (37 kDa) bands. B) E9.5 and C) E10 blot of Gli3 and
870 Gapdh. NAE: Neurulation-stage alcohol exposure; Veh: Lactated Ringer's vehicle group. Each lane
871 represents one pooled litter from the treatment group indicated.

872 **S2 Fig. Representative images of NAE (A) and vehicle-treated (B) embryos 12 hr after exposure**
873 **(E9.5).** No gross morphological differences were observed between the treatment groups at this time
874 point, though volumetric and shape differences of CNS tissue are apparent later in development (11-
875 14). Scale bars = 1 mm.

876 **S3 Fig. NAE causes impairments in rotarod performance in male, but not female, mice.** Male
877 NAE mice, regardless of genotype, had a significantly shorter latency to fall compared to vehicle-
878 treated mice ($F_{(1,48)} = 5.1$; $p = 0.028$). No effect of genotype or treatment on rotarod performance was
879 found in female mice. A main effect of trial was found ($F_{(4,220)} = 24.46$, $p < 0.0001$), demonstrating motor
880 learning in the females across trials. * = $p < 0.05$. For males, n's = 11-15 litters; for females, n's = 13-17
881 litters. Data are shown as group means \pm SEM with each sample representing littermates of each
882 genotype averaged into a single datum.

883 **S4 Fig. Partial loss of cilia motor transport gene *Kif3a* affects behavioral performance on the**
884 **EPM (A-C) and open field (D-F) in adolescent female mice.** For EPM, total arm entries (A) and
885 percent of time (B) in open arms showed no effects of treatment or genotype. However, C) a significant
886 main effect of genotype was revealed for percent of entries into open arms ($F_{(1,57)} = 5.13$, $p = 0.028$),
887 with *Kif3a*^{+/-} female mice making more entries into open arms compared to WT mice. For open field,
888 there was a significant genotype effect (indicated by curved brackets) on horizontal activity (D) ($F_{(1,54)} =$
889 9.2 , $p = 0.004$), center distance (E) ($F_{(1,54)} = 7.9$, $p = 0.007$), center time (F) ($F_{(1,54)} = 6.4$; $p = 0.014$), and
890 repeated beam breaks (S1 Table) ($F_{(1,54)} = 6.7$; $p = 0.013$). Overall, when all time bins were averaged,
891 *Kif3a*^{+/-} female mice were more active and traveled farther in the center of the open field compared to
892 WT females. *Post hoc* analyses were not significant. * = $p < 0.05$, ** = $p < 0.01$.

893 When data were totaled across the session (D-F), Bonferroni *post hoc* tests revealed that Veh *Kif3a*^{+/-}
894 mice had more beam breaks ($p = 0.005$) and center distance traveled ($p = 0.003$) compared to Veh WT
895 mice. For totaled data, significant ($p < 0.05$) *post hoc*s are shown as letters on each graph. a: vs.
896 vehicle-treated WT, b: vs. vehicle-treated *Kif3a*^{+/-}, c: vs. NAE WT. For all groups, n's = 13-17 litters. All
897 data are shown as group means \pm SEM with each sample representing the females from one litter.

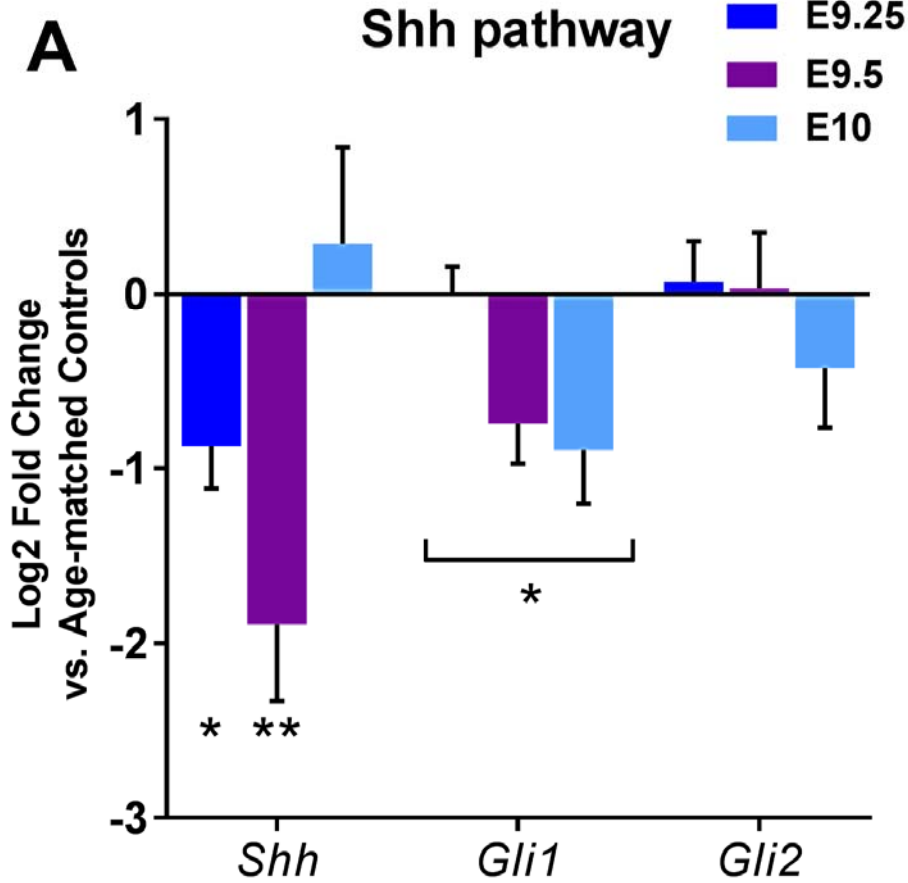
898 **S5 Fig. Partial loss of *Kif3a* reduces brain width and height in adolescent male mice.** A) Neither
899 genotype nor prenatal treatment affected ventricle area. However, B) midline brain width was smaller in

900 both *Kif3a*^{+/-} groups and NAE WT animals compared to vehicle-treated WT mice. C) *Kif3a*
901 heterozygosity also results in smaller medial brain height. * = $p < 0.05$, ** = $p < 0.01$, *** = $p < 0.001$.
902 Group n's = 4-5. All measurements shown as mean + SEM.

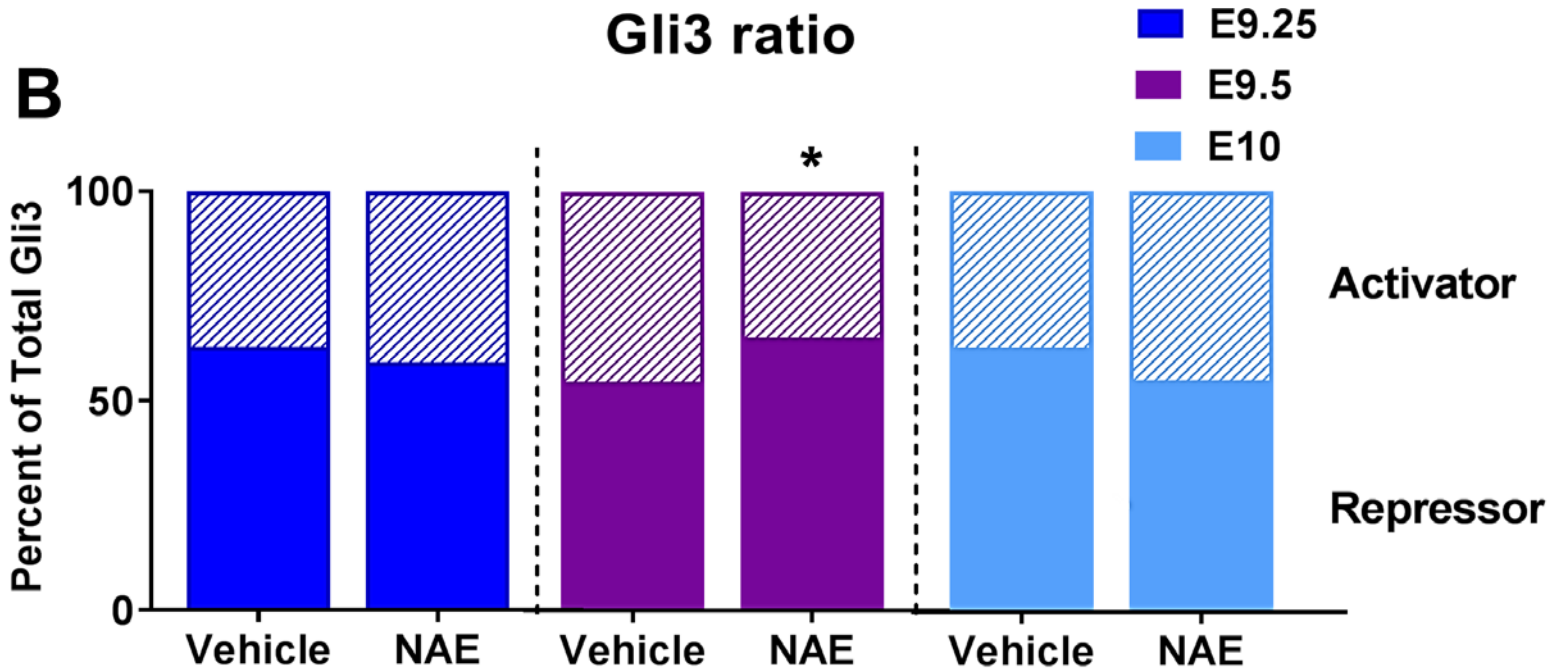
903 **S1 Table. Open field behavioral outcomes in adolescent female *Kif3a*^{+/-} and *Kif3a*^{+/+} mice**
904 **following NAE or vehicle treatment on E9.0.** ^a = Veh *Kif3a*^{+/-} and NAE *Kif3a*^{+/-} (averaged across time
905 bins) significantly differ from the average of Veh WT.

906 **S2 Table. Open field behavioral outcomes in adolescent male *Kif3a*^{+/-} and *Kif3a*^{+/+} mice following**
907 **NAE or vehicle treatment on E9.0.** ^a = Veh *Kif3a*^{+/-} and NAE *Kif3a*^{+/-} (averaged across time bins)
908 significantly differ from the average of Veh WT.

Shh pathway



Gli3 ratio



190 kDa

83 kDa

